Dynamic reconfiguration of frontal brain networks during executive cognition in humans

Urs Braun[a,1], Axel Schäfer[a,1], Henrik Walter[b,1], Susanne Erk[b], Nina Romanczuk-Seiferth[b], Leila Haddad[a], Janina I. Schweiger[a], Oliver Grimm[a], Andreas Heinz[b], Heike Tost[a], Andreas Meyer-Lindenberg[a,1], and Danielle S. Bassett[c,d,1,2]

[a]Central Institute for Mental Health Mannheim, University of Heidelberg, Medical Faculty Mannheim, 68159 Mannheim, Germany; [b]Department of Psychiatry and Psychotherapy, Charité–University Medicine Berlin, Campus Mitte, 10117 Berlin, Germany; [c]Department of Bioengineering, University of Pennsylvania, Philadelphia, PA 19104; and [d]Department of Electrical and Systems Engineering, University of Pennsylvania, Philadelphia, PA 19104

Edited by Marcus E. Raichle, Washington University in St. Louis, St. Louis, MO, and approved July 29, 2015 (received for review December 4, 2014)

The brain is an inherently dynamic system, and executive cognition requires dynamically reconfiguring, highly evolving networks of brain regions that interact in complex and transient communication patterns. However, a precise characterization of these reconfiguration processes during cognitive function in humans remains elusive. Here, we use a series of techniques developed in the field of "dynamic network neuroscience" to investigate the dynamics of functional brain networks in 344 healthy subjects during a working-memory challenge (the "*n*-back" task). In contrast to a control condition, in which dynamic changes in cortical networks were spread evenly across systems, the effortful working-memory condition was characterized by a reconfiguration of frontoparietal and frontotemporal networks. This reconfiguration, which characterizes "network flexibility," employs transient and heterogeneous connectivity between frontal systems, which we refer to as "integration." Frontal integration predicted neuropsychological measures requiring working memory and executive cognition, suggesting that dynamic network reconfiguration between frontal systems supports those functions. Our results characterize dynamic reconfiguration of large-scale distributed neural circuits during executive cognition in humans and have implications for understanding impaired cognitive function in disorders affecting connectivity, such as schizophrenia or dementia.

dynamic network | working memory | graph theory | frontal cortex | flexibility

The era of human brain mapping has demonstrated the power of associating brain regions to specific cognitive functions. However, emerging evidence indicates that many so-called "domain-general" areas engage in multiple functions, differing from "domain-specific" areas such as primary visual cortex that perform a very specific function (1, 2). Such broad engagement is enabled by two fundamental features of brain function: time and interconnectivity. Brain areas and associated circuits or networks may be engaged in tasks differently over time: some transiently and some consistently (2, 3). A fundamental understanding of cognition in general and executive cognition in particular should therefore address the dynamic, interconnected nature of brain function.

Here, we use and extend emerging tools from "dynamic network neuroscience," a field of neuroscientific inquiry that embraces the inherently evolving, interconnected nature of neurophysiological phenomena underlying human cognition (3, 4). Building on the formalism of network science (5), this approach treats the patterns of communication between brain regions as evolving networks and links this evolution to behavioral outcomes. Conceptually, this approach is particularly useful in examining the consistent or transient engagement of neural (or cognitive) circuits or putative functional modules (Fig. 1). We define a network module to be a set of brain regions that are strongly connected to each other and weakly connected to the rest of the network. Using dynamic network-based clustering techniques (6), we seek to observe the flexible recruitment and integration of neural circuits underlying executive function in the form of working memory.

Working memory lies at the interface of perception and action (7) and requires the integration of large-scale neural circuits (8–11). Theoretical frameworks for working memory call on the interplay of distinct components (12) and their integration in broader cognitive circuits (1). The empirical neuroimaging literature has bolstered these conceptualizations by identifying several distinct sets of brain areas underlying working-memory performance (13–17). Nevertheless, a fundamental understanding of the flexible integration and recruitment of these circuits remains incomplete.

In the present study, we characterize the time-dependent interactions between putative neural circuits [network modules (3)] underlying working-memory performance in humans as elicited by an *n*-back task performed during the acquisition of functional MRI (fMRI) data (Fig. 1 *A* and *B*). By deploying a sliding time window analysis (18, 19), we capture brain network dynamics during working-memory function (2-back), during a baseline condition

Significance

Cognitive flexibility is hypothesized to require dynamic integration between brain areas. However, the time-dependent nature and distributed complexity of this integration remains poorly understood. Using recent advances in network science, we examine the functional integration between brain areas during a quintessential task that requires executive function. By linking brain regions (nodes) by their interactions (time-dependent edges), we uncover nontrivial modular structure: groups of brain regions cluster together into densely interconnected structures whose interactions change during task execution. Individuals with greater network reconfiguration in frontal cortices show enhanced memory performance, and score higher on neuropsychological tests challenging cognitive flexibility, suggesting that dynamic network reconfiguration forms a fundamental neurophysiological mechanism for executive function.

Author contributions: U.B. and D.S.B. designed research; U.B. performed research; U.B., A.S., H.W., S.E., N.R.-S., L.H., J.I.S., O.G., A.H., H.T., A.M.-L., and D.S.B. contributed new reagents/analytic tools; U.B. analyzed data; and U.B., H.T., A.M.-L., and D.S.B. wrote the paper.

Conflict of interest statement: H.W. has received speaker fees from Servier. H.W. receives an honorary as editor of Nervenheilkunde. A.M.-L. has received consultant fees and travel expenses from Alexza Pharmaceuticals, AstraZeneca, Bristol-Myers Squibb, Defined Health, Decision Resources, Desitin Arzneimittel, Elsevier, F. Hoffmann–La Roche, Gerson Lehrman Group, Grupo Ferrer, Les Laboratoires Servier, Lilly Deutschland, Lundbeck Foundation, Outcome Sciences, Outcome Europe, PriceSpective, and Roche Pharma and has received speaker fees from Abbott, AstraZeneca, BASF, Bristol-Myers Squibb, GlaxoSmithKline, Janssen-Cilag, Lundbeck, Pfizer Pharma, and Servier Deutschland.

This article is a PNAS Direct Submission.

Freely available online through the PNAS open access option.

[1]U.B., A.S., H.W., A.M.-L., and D.S.B. contributed equally to this work.

[2]To whom correspondence should be addressed. Email: dsb@seas.upenn.edu.

This article contains supporting information online at www.pnas.org/lookup/suppl/doi:10.1073/pnas.1422487112/-/DCSupplemental.

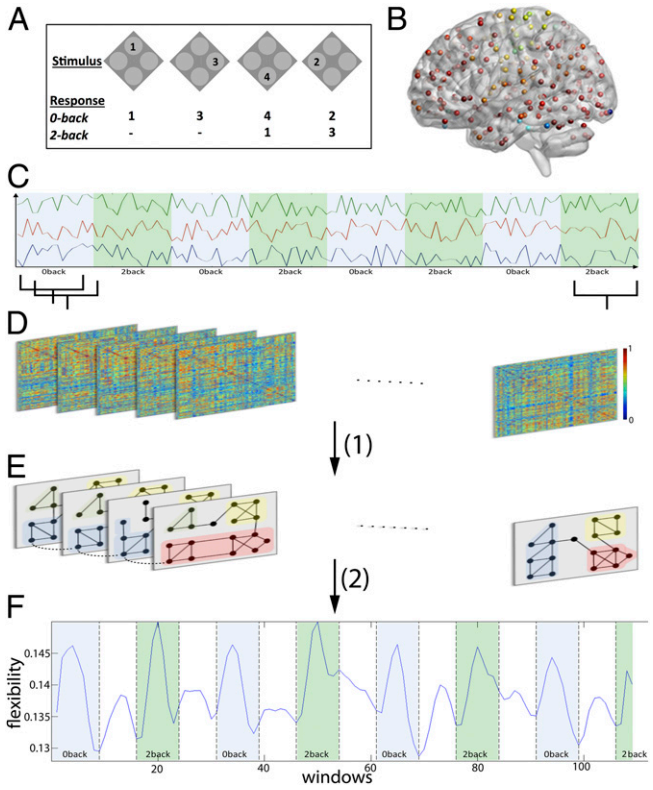

Fig. 1. Network reconfiguration during executive function. (*A*) We use a numerical *n*-back task consisting of 0-back and 2-back conditions. (*B*) We define 270 cortical and subcortical regions of interest (36), and (*C*) extract the mean time course from each region. (*D*) A sliding window comprising 15 volumes with no gap was applied to regional mean time courses, and for each window we estimated the functional connectivity between pairs of regions using coherence. This procedure resulted in a sequence of 114 time-ordered adjacency matrices. (*E*) Using a dynamic community detection algorithm (part 1 in panel), we identified network modules in each time window and tracked their evolution over time. (*F*) By estimating the probability that a brain region changes its allegiance to modules between any two consecutive time windows (part 2 in panel), we observed that whole-brain flexibility oscillated between unitask (2-back or 0-back only) and dual-task (2-back and 0-back in same time window) conditions.

(0-back), and in transitions between baseline and task (Fig. 1 *C* and *D*). We identify putative functional modules in each time window and track how brain regions change their engagement in these modules over time (Fig. 1 *E* and *F*). We quantify those changes over time by flexibility, which measures how often a particular brain region changes its modular allegiance. Based on the cognitive load of the 2-back condition (20–22), we hypothesize that the brain transiently reorganizes functional modules during task performance in comparison with baseline. Furthermore, we hypothesize that this reconfiguration is driven by higher order cognitive control systems, particularly in frontal cortex (2), which are known to play a role in task switching. Finally, based on prior evidence linking network reconfiguration to behavioral adaptation (3), we hypothesize that individuals who display more flexible network structures will perform better than individuals with more rigid network structures.

Results

Dynamics of Flexibility. How do cognitive systems interact as individuals perform a working-memory task? To answer this question, we must understand how network modules form and evolve during task execution. These processes can be revealed using a network-based clustering technique (6) applied to fMRI data acquired during task execution (3, 23–25). We first extracted functional networks from overlapping time windows of fMRI data (*Methods*), and linked networks in consecutive time windows to form a multilayer network (e.g., a network of many time layers), providing important statistical benefits for the estimation of network modules (3, 6). Next, we performed a network-based clustering technique referred to as "dynamic community detection" to extract network modules: each network module corresponded to a set of brain areas that are coherently active in a single time window, forming a putative cognitive system. In essence, a region was assigned to a module composed of regions to which it was most densely connected, and not assigned to a module composed of regions to which it was sparsely connected. The set of fixed assignments of nodes to modules is referred to as a hard partition, and the goodness of this partition is statistically quantified by a modularity quality function (3, 6). Following module extraction, we quantified module evolution throughout the experiment by computing a time-dependent network flexibility: the time-dependent flexibility of a region was defined as the probability that a brain region changed its allegiance to putative functional modules between any two consecutive time windows, and the time-dependent flexibility of a person was defined as the average regional flexibility over all brain areas included in the network. Intuitively, flexibility can be thought of as a statistic to quantify the amount of reconfiguration in functional connectivity patterns that a brain region displays over time.

We observed that the time-dependent network flexibility oscillates across task execution, reaching clear maxima in time windows dominated by either the 2-back or 0-back (baseline) conditions [Fig. 1*F*; repeated-measures ANOVA with condition as factor: $F_{(2,343)} = 20.75$, $P < 0.001$]. This increase in brain-wide flexibility was not modulated by cognitive load: whole-brain flexibility was not significantly different between the 2-back and 0-back conditions [post hoc paired *t* test: $t_{(343)} = 1.31$, $P = 0.19$].

Dynamic Network Reconfiguration. Although the changes in flexibility indicate network reconfiguration dynamics, they do not address the cognitive systems engaged. To uncover these systems and isolate their reconfiguration properties, we next identified the modules of the multilayer networks by distilling a consensus partition of brain regions into network modules that was most representative of all subjects and all times for each level of cognitive load separately (Fig. 2 *A* and *B*). Several modules were consistently identified in both the 0-back and 2-back conditions: somatomotor, visual, subcortical, and hippocampal modules. However, the two conditions differed markedly in frontal-mediated modules (Fig. 2*C*). First, the frontoparietal module was composed of more medial structures in the 0-back condition, and more lateral structures in the 2-back condition; in the 2-back condition, this module also prominently included several regions in the left dorsolateral prefrontal cortex that were missing in the control condition. Second, in the 2-back condition a module consisting of nodes in the right prefrontal cortex dissociated from the bilateral frontotemporal module detected during the 0-back condition. To quantify these results, we compared the consensus partitions for both conditions and each subject separately for frontal and nonfrontal regions using a *z* score of the Rand coefficient (25, 26), which quantifies the similarity between two partitions. A paired *t* test on the *z* score for frontal vs. nonfrontal regions showed a significantly higher similarity for nonfrontal regions [$t_{(343)} = -10.32$, $P < 0.001$], supporting the visually marked differences between frontal and nonfrontal modules.

These findings are conceptually consistent with previous results on the structure of working-memory networks (7, 27) involving frontotemporal and frontoparietal systems, and indicate that a reconfiguration between conditions is most prominent in frontal and frontal-related systems.

We next asked how individual modules differentially reconfigure within both conditions. Each identified cognitive system contributed differently to the observed brain-wide flexibility that dominated

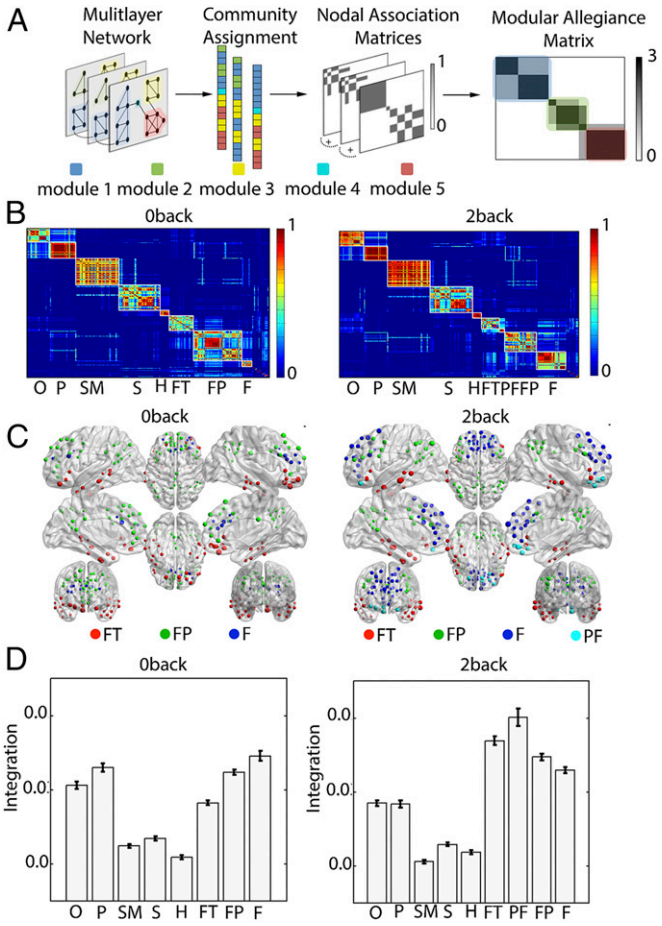

Fig. 2. Evolving network organization. (*A*) To determine whether cognitive systems are transiently or consistently recruited during task execution, we construct a modular allegiance matrix *T* by computing the contingency matrix *N* for each window: the element N_{ij} is equal to 1 if nodes *i* and *j* are in the same module and is equal to zero otherwise. We sum all contingency matrices for each condition to obtain the modular allegiance matrix *T*, whose elements T_{ij} indicate the fraction of time windows in which nodes *i* and *j* have been assigned to the same module. We then apply a community detection algorithm to *T* to obtain a "consensus partition" (25), which represents the common modular structure across all time windows. (*B*) The modular allegiance matrices for the 0-back condition (*Left*) and 2-back condition (*Right*). The letter beneath the block diagonal elements indicates the network module identified in the consensus partition: F, frontal; FP, frontal-parietal; FT, frontotemporal; H, hippocampal; O, occipital; P, parietal; PF, right prefrontal; S, subcortical; SM, somatomotor. (*C*) A mapping of the frontal modules obtained in *B* to their brain coordinates for the 0-back (*Left*) and 2-back condition (*Right*); labels are as in *C*. (*D*) Frontal systems show high integration during 2-back, whereas during 0-back occipital and parietal systems show an equally strong interaction. Error bars indicated SEs of mean over partitions belonging to either to 0-back or 2-back conditions.

0-back and 2-back condition time windows. We calculated the flexibility of each network module in the consensus partition. During the 2-back condition, flexibility was highest in fronto-related systems [repeated-measures ANOVA with modules as categorical factor: $F_{(8,343)} = 29.95$, $P < 0.001$; post hoc paired *t* test between frontal-related and nonfrontal modules: $t_{(343)} = 9.42$, $P < 0.001$]. This pattern was conserved during the 0-back condition [$F_{(7,343)} = 11.75$, $P < 0.001$; post hoc paired *t* test between fronto-related and nonfrontal modules: $t_{(343)} = 4.98$, $P < 0.001$]. However, flexibility was more evenly distributed in the 0-back condition between systems as evidenced by a significant main effect of task and significant interaction in a two-way repeated-measures ANOVA with task and frontal vs. nonfrontal as categorical factors [main effect of task: $F_{(1,343)} = 6.25$, $P < 0.013$; effect of interaction: $F_{(1,343)} = 16.5$, $P < 0.001$]. These finding were robust to variations in the connectivity method (correlation instead of coherence), parameter selection in the community detection algorithm, and changes in the window size (*SI Results*, *Robustness of Results*).

Flexibility can be driven by transient interactions between modules: the more transient module–module interactions, the more likely regions are to flexibly alter their allegiance to cognitive systems. We estimated the transience of module–module interaction by averaging all elements of the module allegiance matrix *T* that link nodes in two different modules; we refer to this quantity as "integration" (24). Consistent with our earlier results, we observed higher integration in frontal systems than nonfrontal systems in the 2-back condition, whereas in the 0-back condition we observed similar integration in both frontal and occipital-parietal systems (Fig. 2*D*). These results suggest that dynamic network reorganization is taking place predominately in frontal systems and is driven by a constant readaptation and interaction of frontal systems with each other.

Role of Frontal Systems in Executive Functioning. Based on our finding that whole-brain flexibility is driven by reconfiguration of and between fronto-related systems, we explored the relationship between frontal flexibility and cognitive performance. We used an α-level of 0.05 for all statistical tests and report both false-discovery rate (FDR) and Bonferroni-corrected *P* values. We interpret results that do not pass Bonferroni correction as exploratory. During the 2-back working-memory condition, frontal flexibility was positively correlated with task accuracy (Fig. 3*A*; Spearman's rank correlation coefficient $r = 0.12$, $P_{\text{FDR-corrected}} = 0.04$, $P_{\text{Bonferroni}} = 0.2$), supporting the conclusion that higher frontal flexibility is cognitively beneficial for working-memory performance.

As noted in the previous section, an important driver of flexibility is the strength of module–module integration, which can be used to

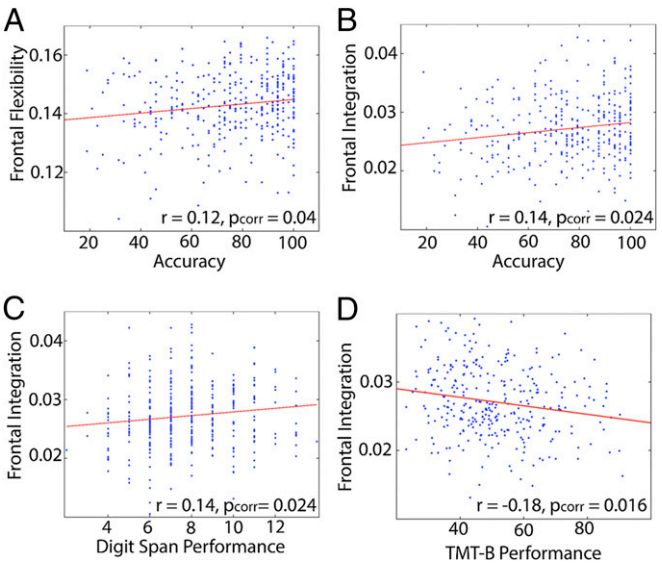

Fig. 3. Role of frontal systems in executive functioning. (*A*) The flexibility in the frontal cortex during 2-back is positively correlated with 2-back task accuracy, measured in percentage of right answers. (*B*) Integration, as the contribution to flexibility that is due to between-module reconfiguration, shows an even stronger association with task accuracy. (*C* and *D*) Furthermore, frontal integration is related to other cognitive measures as shown by correlation with the performance in the digit span test (backward, measured in number of correctly remembered items) and the performance in the trail-making test B (TMT-B, measured in seconds to task completion).

quantify transient interactions between cognitive systems and which is conceptually related to posited drivers of prefrontal function in working memory (28). We hypothesized that executive function stems from the structured interaction between large-scale frontal systems. To test this hypothesis, we next evaluated the relationship between the reconfiguration of frontal systems (measured by integration) and behavior (measured by task performance and neuropsychological test scores), thereby exploring the link between integration during the 2-back task and working-memory performance. During the 2-back condition, frontal integration was positively correlated with task accuracy (Fig. 3*B*; Spearman's rank correlation coefficient $r = 0.14$, $P_{\text{FDR-corrected}} = 0.024$, $P_{\text{Bonferroni}} = 0.096$), suggesting that the ability to easily switch between modules or brain states is essential for working-memory performance.

Our results could support (*i*) frontal integration is required for 2-back working-memory accuracy alone, or (*ii*) frontal integration is required for working-memory performance more generally. To distinguish these scenarios, we tested the relationship between frontal integration and performance on a digit span backward task, which captures temporary information storage and the active manipulation of stored items. The digit span backward task engages the frontal lobe more strongly than the digit span forward task (27), which does not require active information manipulation. We examined both digit span measures and observed that frontal integration was positively correlated with backward digit span score (Fig. 3*C*; $r = 0.14$, $P_{\text{FDR-corrected}} = 0.024$, $P_{\text{Bonferroni}} = 0.072$) but not the forward digit span score (Spearman's rank correlation coefficient $r = 0.004$, $P_{\text{FDR-corrected}} = 0.95$, $P_{\text{Bonferroni}} = 1.0$). This indicates that the dynamic reconfiguration of frontal systems for working-memory function may not be limited to the *n*-back working-memory paradigm but may be essential for the manipulation of stored information across tasks.

The relationship between frontal integration and an external measure of working-memory function that challenges active information manipulation suggests the possibility that reconfiguration of frontal systems could form a critical mechanism for executive function more generally, specifically in its utilization of cognitive flexibility. We directly tested the relationship between frontal integration and cognitive flexibility using behavioral scores on the trail-making test B (TMT-B), which measures executive flexibility by capturing the subject's cognitive ability to switch between task demands. A large score on the TMT-B task (as measured by the time to complete the task) indicates poor task switching ability, and a small score indicates good task switching ability. We observed that frontal integration was negatively correlated with TMT-B performance (Fig. 3*D*; Spearman's rank correlation coefficient $r = -0.18$, $P_{\text{FDR-corrected}} = 0.016$, $P_{\text{Bonferroni}} = 0.016$), suggesting that the ability of the frontal cortex to switch between network modules (as a measure of switching between functional states) is a more general feature of cognitive functioning rather than being specific to working-memory function.

Taken together, our results suggest that working memory requires the active and dynamic reconfiguration of large-scale brain systems driven by frontal networks. Interactions between these frontal systems might underlie executive function more generally.

Discussion

As a complex system, the human brain is intrinsically organized into modules, creating a high degree of flexibility and adaptability of the system without fundamentally altering underlying structure (29, 30). However, this modular structure is not static but undergoes changes in response to external and internal drivers, ranging from cognitive processes (3, 31) to disease (32).

In the present study, we have provided evidence that the functional connectivity during a working-memory task is dynamically organized into adapting modules and that this adapting modular structure relates to cognitive demands. We quantified the amount of this adaption using a previously undefined time-dependent network flexibility measure, an intuitive statistic summarizing reconfiguration within and between brain systems. We provide evidence that the amount of reorganization in the modular structure and specifically the amount of interaction between modules is behaviorally relevant to working-memory performance and cognitive flexibility. Our results provide support for the emerging paradigm of cognitive functions as a dynamic orchestration of distributed cognitive networks.

Task-Based Dynamics of Flexibility. Network flexibility has previously been linked to behaviorally advantageous changes in brain network dynamics in response to cognitive demands by predicting individual differences in learning (3) and by offering a network mechanism of cognitive control over many tasks (31). In the current study, we demonstrate that brain network flexibility and its relationship to cognitive demand can be tracked continuously on the order of minutes and undergoes specific and repetitive changes even within a given task. Although prior studies have focused exclusively on task-related (vs. task-unrelated) aspects of connectivity using methods such as psychophysiological interaction (33), our work focuses on the temporal dynamics of the networks underlying working-memory performance. Using a previously undefined measure of time-dependent network flexibility, we show that the brain reconfigures in an oscillatory manner as participants switch between different task conditions, suggesting that reconfiguration of brain networks tracks brain state transitions, even when both brain states (task conditions) display equivalent flexibility.

Despite the conservation of whole-brain flexibility across working-memory load, we did observe a redistribution of flexibility across cognitive systems. Flexibility is greater in frontal systems in the 2-back condition as opposed to the 0-back condition, consistent with other recent studies using different tasks (23, 31, 33), adding evidence for a domain-general role of these systems. Moreover, this increase in reconfiguration is accompanied by a reorganization of network modules: frontal-related modules show a different organization between tasks, most noticeably a strong medial module during 0-back, and a dissociation of prefrontal nodes from a frontotemporal network during 2-back. The latter dissociation is reminiscent of the altered functional coupling of prefrontal areas commonly observed in *n*-back studies, which has been shown to be altered in disease states (17, 34), and which has been argued to be under some genetic control (35).

Flexibility atop a Conserved Modular Backbone. The flexibility of network configurations during the *n*-back task occur on top of a highly conserved modular backbone. We observe that functional connectivity patterns display strong community structure, as evidenced by the block-diagonal structure of the module allegiance matrices represented in Fig. 2*B*. The segregation of network modules observed in this data is much more pronounced than that observed in resting-state functional connectivity matrices (23, 36, 37). The identified network modules map well to biologically meaningful systems of intrinsic connectivity (36) and specifically systems commonly engaged during working-memory performance (14, 38, 39) (see *Supporting Information* for a quantitative comparison with refs. 36 and 39). Moreover, this modular structure is relatively conserved across task states: in fact, nonfrontal modules including visual and somatomotor modules are identical in node composition in 0-back and 2-back conditions. These highly stable modules also display relatively low flexibility across both *n*-back task conditions (*Supporting Information*), suggesting that they form a stable task-based core that supports higher order cognitive functions (40). Indeed, the combination of flexible reconfiguration and a conserved modular backbone is consistent with the task-based core-periphery structure of the human connectome (40), which has been posited to enable both the stability necessary for successful task performance and the flexibility necessary for behavioral adaptation.

Integration Between Cognitive Modules. The simultaneous existence of flexible reconfiguration and a conserved modular structure is made possible by time-dependent integration between cognitive modules. As modules become more integrated, regions can change their allegiance to modules more quickly, potentially forming bridges of communication. Critically, we observe that network modules differ in their degree of integration with other network modules: stable core-like modules including visual and somatomotor systems show relatively weak integration with other modules, whereas frontal and frontal-mediated modules show relatively strong integration with other modules (Fig. 2*D*). This finding is consistent with prior work from Fornito et al. (33), showing that the frontal network displays extensive cooperation during task execution, and further complements a recent study from Cole et al. (31) demonstrating that the frontoparietal network displays a high variance in connectivity over different tasks (*Supporting Information*).

The large variation in integration across these modules suggests that cognitive systems play different roles in executive function predicated on the degree of interconnectivity with other systems. It is intuitively plausible that the strong integration of frontal systems with other network modules forms a physiological basis for cognitive flexibility (15, 41), enabling task switching and cognitive control during demanding tasks (21, 42).

Behavioral Relevance of Flexibility and Integration. Using FDR correction methods for multiple-comparisons testing, we observed that frontal flexibility and integration were correlated with working-memory accuracy during the 2-back condition. As exploratory findings, some of which did not pass Bonferroni correction, these dynamic network correlates of behavior complement and extend prior observations from static network analyses (43–45). The specificity of these correlations to the frontal systems suggests that network reconfiguration may form a putative neurophysiological mechanism of cognitive flexibility and executive function more generally (16). Indeed, this hypothesis is supported by the fact that frontal integration was associated with both the backward digit span scores (measuring active information manipulation) and TMT-B scores (measuring executive flexibility), further highlighting the critical importance of intersystem connectivity in the successful execution of more cognitively demanding tasks.

Methodological Limitations. Our findings are subject to several methodological considerations. First, we use a dynamic community detection algorithm to cluster brain regions into coherently activated communities. However, due to heuristics in the algorithm and challenges inherent to fMRI data, the assignment of nodes to communities on the individual subject level remains a statistical process, accompanied by some degree of uncertainty. Second, although we aim at a description of dynamic reconfiguration, we remain limited by the temporal resolution of fMRI data, making it likely that the modular changes and behavioral associations we observed might be further resolved in time if electrophysiological data were used. Third, we use a measure of functional connectivity that does not reflect causal interaction. Future studies might benefit from using model-based methods for effective connectivity such as dynamic causal modeling or structural equation modeling to estimate causal interactions between a smaller subsets of brain regions. Fourth, we study a hard partition of nodes into communities, which has the advantage of providing a parsimonious estimate of the module allegiance matrix that is robust to noisy measurements of functional connectivity between brain regions. Should soft partitioning methods be extended to temporal networks, they might provide complementary insights into the nature of changing community assignments. Fifth, although the *n*-back task is a well-studied manipulation of working-memory capacity, the structure of the task makes it difficult to distinguish the cognitive subprocesses of working-memory maintenance and information manipulation (46). Finally, the behavioral correlations we observed are small and some fail to reach statistical significance under Bonferroni correction, and therefore should be interpreted with caution and validated in future studies. However, these relationships do explain additional variance in comparison with more traditional approaches, highlighting the importance of small contributions to the highly complex phenotype of brain network dynamics.

Conclusions

Here we characterize the dynamic nature of neural processes during working-memory performance, which stems from the reconfiguration of large-scale distributed neural circuits rather than from the activity of isolated brain areas. Starting from a data-driven approach to cluster brain regions into communities, we track changes in network reconfiguration to frontal-related systems and show that the adaptive nature of the frontal cortex is relevant for cognitive functioning. Our study demonstrates the power of dynamic network neuroscience approaches to the study of cognition and behavior in humans. A better characterization of how dynamic reconfiguration of networks relates to cognition should also advance our understanding of disorders in which prominent cognitive disturbance arises from developmental (e.g., autism or schizophrenia) or degenerative pathologies (e.g., dementia).

Methods

Participants, Data Acquisition, and Preprocessing. For a group of 344 healthy volunteers (180 women; mean age, 33; range, 18–51 y) as part of a multicenter study (35), blood oxygen level-dependent fMRI was acquired while subjects were performing the *n*-back task. All participants provided written informed consent for protocols approved by the institutional review boards of the Medical Faculty Mannheim of the University of Heidelberg, the Medical Faculty of the University of Bonn, and the Charité–University Medicine Berlin. Data were preprocessed according to standard protocols as previously described in refs. 47 and 48. After preprocessing, the mean time series in 5-mm spheres around coordinates defined by ref. 36 were extracted. For reasons of brain coverage, six additional coordinates were added based on metaanalytical studies. After applying a sliding time window with the length of 15 volumes and no gap between windows as suggested by Leonardi et al. (49), we used the Morlet wavelet transform to estimate the functional connectivity between each pair of brain regions in the frequency interval 0.08–0.15 Hz, as described previously (3). For each subject, this procedure yielded 114 weighted adjacency matrices describing the functional connectivity in each time window.

Identifying Putative Functional Modules. For each subject, the resulting matrices were partitioned into time-respecting modules using a multilayer community detection algorithm introduced in the study by Mucha et al. (6) and first applied to neuroimaging data in ref. 3. Due to heuristics in the algorithm and near degeneracy of the modularity landscape, individual runs of the algorithms could produce slightly different partitions of nodes into modules. As a common approach to dealing with this degeneracy, we repeated the modularity estimation 100 times for each subject (25). For each repetition, we calculated the flexibility change matrix F, whose binary elements $F_{i,j}$ indicate if node i changes its module between two consecutive time windows. Averaging over all repetitions, we obtain the flexibility matrix for each subject, whose elements indicate the probability that a brain region changes its allegiance to putative functional modules between any two consecutive time windows.

Consensus Partitions and Integration. To find a consensus partition that is most representative of the underlying community structure, we applied a consensus algorithm as described in detail in ref. 25. In short, to find a consensus partition S that is most representative of a number n of given partitions $C_1, C_2, \ldots, C_n$, we computed for each partition $C_1, C_2, \ldots, C_n$ its modular allegiance matrix T whose binary elements T_{ij} indicate if two nodes i and j have been assigned to the same module or not. Summing up all modular allegiance matrices, we obtained the consensus matrix T_{cons}, the elements of which indicate how often two nodes have been assignment to the same module. To account for noise, only elements whose assignments were higher than in an appropriate random null model were taken into account. By running a community detection algorithm on the

consensus matrix T_{cons}, we obtained a consensus partition S that is most representative of the underlying structure in the initial partitions.

Further details on the methods and materials can be found in *Supporting Information*.

ACKNOWLEDGMENTS. D.S.B. acknowledges support from the John D. and Catherine T. MacArthur Foundation, the Alfred P. Sloan Foundation, the Army Research Laboratory through Contract W911NF-10-2-0022 from the US Army Research Office, the Institute for Translational Medicine and Therapeutics at Penn, the National Institute of Mental Health through Award 2-R01-DC-009209-11 (Thompson-Schill), and National Science Foundation Awards BCS-1441502 and BCS-1430087 through the Engineering, Computer and Information Science and Engineering, and Social, Behavioral, and Economic Sciences Directorates. This study was supported by the German Federal Ministry of Education and Research [Bundesministerium für Bildung und Forschung (BMBF)] through the Integrated Genome Research Network Systematic Investigation of the Molecular Causes of Major Mood Disorders and Schizophrenia [Grants 01GS08144 (to H.W.), 01GS08147 (to A.M.-L.), and 01GS08148 (to A.H.)]. A.M.-L. acknowledges support from Novel Methods Leading to New Medications in Depression and Schizophrenia—the work leading to these results has received funding from the Innovative Medicines Initiative Joint Undertaking under Grant Agreement 115008. H.T. gratefully acknowledges grant support by the German Federal Ministry of Education and Research (BMBF 01GQ1102).

1. Shohamy D, Turk-Browne NB (2013) Mechanisms for widespread hippocampal involvement in cognition. *J Exp Psychol Gen* 142(4):1159–1170.
2. Fedorenko E, Thompson-Schill SL (2014) Reworking the language network. *Trends Cogn Sci* 18(3):120–126.
3. Bassett DS, et al. (2011) Dynamic reconfiguration of human brain networks during learning. *Proc Natl Acad Sci USA* 108(18):7641–7646.
4. Muldoon SF, Bassett DS (2014) Why network neuroscience? Compelling evidence and current frontiers. Comment on "Understanding brain networks and brain organization" by Luiz Pessoa. *Phys Life Rev* 11(3):455–457.
5. Holme P, Saramäki J (2012) Temporal networks. *Phys Rep* 519(3):97–125.
6. Mucha PJ, Richardson T, Macon K, Porter MA, Onnela JP (2010) Community structure in time-dependent, multiscale, and multiplex networks. *Science* 328(5980):876–878.
7. Linden DE (2007) The working memory networks of the human brain. *Neuroscientist* 13(3):257–267.
8. Shrager Y, Levy DA, Hopkins RO, Squire LR (2008) Working memory and the organization of brain systems. *J Neurosci* 28(18):4818–4822.
9. Bressler SL, Menon V (2010) Large-scale brain networks in cognition: Emerging methods and principles. *Trends Cogn Sci* 14(6):277–290.
10. Dehaene S, Naccache L (2001) Towards a cognitive neuroscience of consciousness: Basic evidence and a workspace framework. *Cognition* 79(1-2):1–37.
11. Baars BJ, Franklin S (2003) How conscious experience and working memory interact. *Trends Cogn Sci* 7(4):166–172.
12. Baddeley A (1998) Working memory. *C R Acad Sci III* 321(2-3):167–173.
13. Baddeley A (2003) Working memory: Looking back and looking forward. *Nat Rev Neurosci* 4(10):829–839.
14. Ginestet CE, Simmons A (2011) Statistical parametric network analysis of functional connectivity dynamics during a working memory task. *Neuroimage* 55(2):688–704.
15. Collette F, Van der Linden M (2002) Brain imaging of the central executive component of working memory. *Neurosci Biobehav Rev* 26(2):105–125.
16. McNab F, Klingberg T (2008) Prefrontal cortex and basal ganglia control access to working memory. *Nat Neurosci* 11(1):103–107.
17. Deserno L, Sterzer P, Wüstenberg T, Heinz A, Schlagenhauf F (2012) Reduced prefrontal-parietal effective connectivity and working memory deficits in schizophrenia. *J Neurosci* 32(1):12–20.
18. Liu X, Duyn JH (2013) Time-varying functional network information extracted from brief instances of spontaneous brain activity. *Proc Natl Acad Sci USA* 110(11): 4392–4397.
19. Hutchison RM, et al. (2013) Dynamic functional connectivity: Promise, issues, and interpretations. *Neuroimage* 80:360–378.
20. Baddeley A (1996) Exploring the central executive. *Q J Exp Psychol A* 49(1):5–28.
21. Miyake A, et al. (2000) The unity and diversity of executive functions and their contributions to complex "Frontal Lobe" tasks: A latent variable analysis. *Cognit Psychol* 41(1):49–100.
22. Kane MJ, Conway AR, Miura TK, Colflesh GJ (2007) Working memory, attention control, and the *N*-back task: A question of construct validity. *J Exp Psychol Learn Mem Cogn* 33(3):615–622.
23. Cole MW, Bassett DS, Power JD, Braver TS, Petersen SE (2014) Intrinsic and task-evoked network architectures of the human brain. *Neuron* 83(1):238–251.
24. Bassett DS, Yang M, Wymbs NF, Grafton ST (2014) Learning-induced autonomy of sensorimotor systems. arXiv:1403.6034.
25. Bassett DS, et al. (2013) Robust detection of dynamic community structure in networks. *Chaos* 23(1):013142.
26. Traud AL, Kelsic ED, Mucha PJ, Porter MA (2011) Comparing community structure to characteristics in online collegiate social networks. *SIAM Rev* 53(3):526–543.
27. Owen AM, Lee AC, Williams EJ (2000) Dissociating aspects of verbal working memory within the human frontal lobe: Further evidence for a "process-specific" model of lateral frontal organization. *Psychobiology (Austin Tex)* 28(2):146–155.
28. Miller EK, Cohen JD (2001) An integrative theory of prefrontal cortex function. *Annu Rev Neurosci* 24:167–202.
29. Kirschner M, Gerhart J (1998) Evolvability. *Proc Natl Acad Sci USA* 95(15):8420–8427.
30. Bassett DS, Gazzaniga MS (2011) Understanding complexity in the human brain. *Trends Cogn Sci* 15(5):200–209.
31. Cole MW, et al. (2013) Multi-task connectivity reveals flexible hubs for adaptive task control. *Nat Neurosci* 16(9):1348–1355.
32. Alexander-Bloch AF, et al. (2010) Disrupted modularity and local connectivity of brain functional networks in childhood-onset schizophrenia. *Front Syst Neurosci* 4:147.
33. Fornito A, Harrison BJ, Zalesky A, Simons JS (2012) Competitive and cooperative dynamics of large-scale brain functional networks supporting recollection. *Proc Natl Acad Sci USA* 109(31):12788–12793.
34. Meyer-Lindenberg A, et al. (2001) Evidence for abnormal cortical functional connectivity during working memory in schizophrenia. *Am J Psychiatry* 158(11): 1809–1817.
35. Esslinger C, et al. (2009) Neural mechanisms of a genome-wide supported psychosis variant. *Science* 324(5927):605.
36. Power JD, et al. (2011) Functional network organization of the human brain. *Neuron* 72(4):665–678.
37. Meunier D, Achard S, Morcom A, Bullmore E (2009) Age-related changes in modular organization of human brain functional networks. *Neuroimage* 44(3):715–723.
38. Hampson M, Driesen NR, Skudlarski P, Gore JC, Constable RT (2006) Brain connectivity related to working memory performance. *J Neurosci* 26(51):13338–13343.
39. Owen AM, McMillan KM, Laird AR, Bullmore E (2005) *N*-back working memory paradigm: A meta-analysis of normative functional neuroimaging studies. *Hum Brain Mapp* 25(1):46–59.
40. Bassett DS, et al. (2013) Task-based core-periphery organization of human brain dynamics. *PLoS Comput Biol* 9(9):e1003171.
41. Stuss DT (2006) Frontal lobes and attention: Processes and networks, fractionation and integration. *J Int Neuropsychol Soc* 12(2):261–271.
42. Dosenbach NU, Fair DA, Cohen AL, Schlaggar BL, Petersen SE (2008) A dual-networks architecture of top-down control. *Trends Cogn Sci* 12(3):99–105.
43. Palva JM, Monto S, Kulashekhar S, Palva S (2010) Neuronal synchrony reveals working memory networks and predicts individual memory capacity. *Proc Natl Acad Sci USA* 107(16):7580–7585.
44. Roux F, Wibral M, Mohr HM, Singer W, Uhlhaas PJ (2012) Gamma-band activity in human prefrontal cortex codes for the number of relevant items maintained in working memory. *J Neurosci* 32(36):12411–12420.
45. Cohen JR, Gallen CL, Jacobs EG, Lee TG, D'Esposito M (2014) Quantifying the reconfiguration of intrinsic networks during working memory. *PLoS One* 9(9):e106636.
46. Krieger S, et al. (2005) Executive function and cognitive subprocesses in first-episode, drug-naive schizophrenia: An analysis of *N*-back performance. *Am J Psychiatry* 162(6): 1206–1208.
47. Cao H, et al. (2014) Test-retest reliability of fMRI-based graph theoretical properties during working memory, emotion processing, and resting state. *Neuroimage* 84:888–900.
48. Plichta MM, et al. (2012) Test-retest reliability of evoked BOLD signals from a cognitive-emotive fMRI test battery. *Neuroimage* 60(3):1746–1758.
49. Leonardi N, Van De Ville D (2015) On spurious and real fluctuations of dynamic functional connectivity during rest. *Neuroimage* 104:430–436.
50. Jutla I, Jeub L, Mucha P (2011) A generalized Louvain method for community detection implemented in MATLAB (computer program). Available at netwiki.amath.unc.edu. Accessed September 1, 2014.
51. Good BH, de Montjoye Y-A, Clauset A (2010) Performance of modularity maximization in practical contexts. *Phys Rev E Stat Nonlin Soft Matter Phys* 81(4 Pt 2):046106.
52. Lederbogen F, et al. (2011) City living and urban upbringing affect neural social stress processing in humans. *Nature* 474(7352):498–501.
53. Amthauer R, Brocke B, Liepmann D, Beauducel A (1999) *Intelligenz-Struktur-Test 2000: IST 2000* (Hogrefe and Huber, Göttingen, Germany).
54. Franzen MD, Paul D, Iverson GL (1996) Reliability of alternate forms of the trail making test. *Clin Neuropsychol* 10(2):125–129.
55. Spreng RN, Mar RA, Kim AS (2009) The common neural basis of autobiographical memory, prospection, navigation, theory of mind, and the default mode: A quantitative meta-analysis. *J Cogn Neurosci* 21(3):489–510.
56. Liu X, Hairston J, Schrier M, Fan J (2011) Common and distinct networks underlying reward valence and processing stages: A meta-analysis of functional neuroimaging studies. *Neurosci Biobehav Rev* 35(5):1219–1236.
57. Sabatinelli D, et al. (2011) Emotional perception: Meta-analyses of face and natural scene processing. *Neuroimage* 54(3):2524–2533.
58. Breakspear M, Heitmann S, Daffertshofer A (2010) Generative models of cortical oscillations: Neurobiological implications of the kuramoto model. *Front Hum Neurosci* 4:190.
59. Doron KW, Bassett DS, Gazzaniga MS (2012) Dynamic network structure of interhemispheric coordination. *Proc Natl Acad Sci USA* 109(46):18661–18668.
60. Medaglia JD, Lynall ME, Bassett DS (2015) Cognitive network neuroscience. *J Cogn Neurosci* 27(8):1471–1491.
61. Bassett DS, Yang M, Wymbs NF, Grafton ST (2015) Learning-induced autonomy of sensorimotor systems. *Nat Neurosci* 18(5):744–751.
62. Yeo BT, et al. (2011) The organization of the human cerebral cortex estimated by intrinsic functional connectivity. *J Neurophysiol* 106(3):1125–1165.

Supporting Information

Braun et al. 10.1073/pnas.1422487112

SI Results

Distribution of Integration and Flexibility in the Brain. Although we did not detect any differences in the whole-brain average flexibility between the two task conditions, we did observe differences in the distribution of regional flexibility values across the brain. For each putative module identified on the group level, we computed each module's flexibility by calculating the mean of the regional flexibilities of all nodes in that particular module for each subject individually. The observed network modules displayed significantly different flexibility in both task conditions [repeated-measures ANOVA with modules as factor: 0-back: $F_{(7,343)} = 11.75$, $P < 0.001$; 2-back: $F_{(8,343)} = 29.95$, $P < 0.001$], as shown in Fig. S1. In both task conditions, nodes in frontal modules showed an increased flexibility in comparison with the rest of the brain [paired t test, frontal vs. nonfrontal regions: 0-back: $t_{(343)} = 4.98$, $P < 0.001$; 2-back: $t_{(343)} = 9.42$, $P < 0.001$]. Interestingly, when comparing flexibility between 0-back and 2-back conditions in the anatomically defined frontal regions, we found a significant difference [paired t test, frontal flexibility during 0-back vs. frontal flexibility during 2-back: $t_{(343)} = 2.0$, $P = 0.045$]. These results suggest that flexibility shifts toward frontal systems in response to increasing cognitive demands.

As noted in the main manuscript, flexibility can be driven by transient interactions between modules: the more transient module–module interactions, the more likely regions are to flexibly alter their allegiance to cognitive systems—an aspect of reconfiguration that we capture by integration. However, changes in transient module–modules interactions might also be due to spurious fluctuations in connectivity between regions that do not represent task-related aspects of interaction. To demonstrate that the variation in integration of different modules is indeed driven by real rather than spurious interactions, we permuted the labels of each consensus matrix, applied the community detection algorithm, calculated the integration of each node separately, and repeated this procedure 1,000 times. Averaging the integration of each node for each repetition over the originally identified modules, should yield a null distribution, as shown in Fig. S2 (black columns indicate original data; gray columns indicate integration from 1,000 iterations; error bars indicate SD over 1,000 iterations; left panel corresponds to 0-back, and right panel corresponds to 2-back). This analysis confirms our previous results are not due to noise and finite data length, but show task-specific variations.

Robustness of Results.

Parameter selection. As described in *SI Methods* in detail, the multilayer community detection algorithm requires the selection of two different parameters—ω and γ—that tune the resolution of the community structure (γ) and the strength of interlayer coupling (ω). As a standard and in absence of an a priori hypothesis, those parameters are normally set to 1. However, to demonstrate that our results are robust to a different selection of those parameters, we reanalyzed our data with different parameter values (γ ranging from 0.95 to 1.05 and ω ranging from 0.95 to 1.05), obtaining qualitatively similar results.

Functional connectivity metric. Consistent with our prior work, we have chosen to use a wavelet-based coherence over the Pearson correlation coefficient for statistical, mathematical, and computational reasons. Statistically, the wavelet-based coherence is much more robust to outliers in the data than the Pearson correlation coefficient, which can be extremely sensitive to movement-related artifacts. Mathematically, the wavelet-based measures provide significant denoising to the signal, enhancing signal-to-noise ratio in subsequent analyses. Computationally, our choice of coherence was motivated by the advantage that coherence scales the dependence of two signals in the range of 0–1, thereby (*i*) avoiding negative correlations whose interpretation is debated, and (*ii*) avoiding the need for a doubling of resolution parameter choices in the community detection analysis (a set for positive connections, and a set for negative connections).

However, for completeness, we repeated our analysis with a different measure of functional connectivity: the Pearson correlation coefficient. Using this approach, we observed qualitatively similar results. First, we again saw that network flexibility displays an oscillatory pattern across the experiment. Second, we again observed that frontal regions were more flexible than nonfrontal regions [repeated-measures ANOVA with (*i*) task and (*ii*) frontal vs. nonfrontal as categorical factors: main effect of frontal vs. nonfrontal, $F_{(1,343)} = 64.6$, $P < 0.001$]. Third, we observed that the decomposition of the module allegiance matrices into network modules was replicable. Fourth, we observed a significant difference in flexibility between 0-back and 2-back [repeated-measures ANOVA with task and frontal vs. nonfrontal as categorical factors, main effect of task: $F_{(1,343)} = 21.8$, $P < 0.001$], which was a trend in the results based on coherence.

Choice of time window. To further validate the robustness of our results, we next addressed the question of time windows used to construct the functional connectivity matrices. In a recent paper from Van De Ville and colleague (49), the authors demonstrate the optimality of a 30-s time window for quantifying dynamic reconfiguration of networks in the frequency range 0.08–0.15 Hz. In our work, we adhere to this suggested methodological choice, and use windows of size 15 volumes [or 30 s with a repetition time (TR) of 2 s]. A serendipitous consequence of this choice is that we were also able to have at least one window per block composed exclusively of either 0-back or 2-back data (block length, 30 s). Thus, our choice of window size is in line with state of the art methods for uncovering dynamic functional connectivity in neuroimaging [blood oxygen level-dependent (BOLD)] data.

However, to demonstrate the robustness of our finding to small variation in this choice, we performed two additional analyses. First, we calculated the Pearson correlation coefficient between the coherence matrix extracted from one window, and the coherence matrix extracted from the subsequent window. As the overlap of the time series is large (14/15 volumes = 91%), we would expect the coherence matrices to show significant correlations if they were sensitive to biologically meaningful processes rather than random noise. Indeed, the mean correlation coefficient between consecutive coherence matrices (constructed from windows of size 15 TRs) was $r = 0.81$. These results indicate that window sizes of 15 TRs can robustly uncover reliable network architectures in this experimental context. In a second analysis, we repeated our computations for the shorter window size of 14 volumes. We robustly observe that network flexibility oscillates across task performance, and we further reliably find that frontal regions are more flexible than nonfrontal regions [two-way repeated-measures ANOVA with (*i*) task and (*ii*) frontal vs. nonfrontal as categorical factors: main effect of frontal vs. nonfrontal, $F_{(1,343)} = 196.8$, $P < 0.001$]. Together, this set of additional analyses suggests that our results are relatively robust to small variation in methodological choices.

Degeneracy of Modularity Landscape. As stated in *SI Methods*, maximizing the modularity quality function is NP-hard, and we therefore use a Louvain-like locally greedy heuristic algorithm

(50) to seek the optimal modularity index Q. Methods for dealing with the near degeneracy of the modularity quality function are currently under development (25, 51), and the optimal choices may evolve over the next several years. However, as of today, a common method for dealing with this degeneracy is to examine statistics averaged over the 100 repetitions of the optimization, with equal weight being placed on each solution, rather than just on the unique solutions. The reason for this is that the heuristic begins the optimization in a different part of the modularity landscape. Therefore, identical solutions that are obtained from diverse initial conditions actually indicate important replicable features of the landscape, which should be accounted for in subsequent analysis. Thus, each solution (rather than unique solutions only) is given equal weight in the average.

Comparisons of Our Flexible Community Structure to Recent Findings. To quantify the overlap of the network communities identified in this data to those identified in previous studies, we further compared our module assignments to recent community-based decompositions extracted from resting-state data (36). From these calculations, we observe that the module that we have referred to as the "parietal module" contains a large portion of higher-order association areas that were classified as part of the visual system in Power et al. (36) (i.e., 85% of nodes in our parietal module were assigned to Power et al.'s "visual module"), and that the module that we have referred to as the "subcortical module" incorporates brain regions affiliated with both Power's subcortical and auditory modules. These differences are consistent with the fact that we examine community structure in module allegiance matrices, which are sensitive to fewer larger modules, as opposed to single-subject functional connectivity matrices, which are sensitive to a larger number of smaller modules. All modules and their corresponding decomposition from ref. 36 can be found in Tables S1 and S2.

In addition, we performed a quantitative analysis to compare our network flexibility metric (defined from community detection) to the conceptually similar variance in connectivity over tasks used in the study by Cole et al. (31). In our data, we observed that frontoparietal networks showed higher flexibility than the mean flexibility of the rest of the brain [paired t test between the network flexibility of the frontoparietal network vs. the network flexibility of the remainder of the brain: $t_{(343)} = 6.97$, $P < 0.001$]. This is consistent with Cole et al.'s finding that the frontoparietal system displayed a high variance in connectivity over tasks. Interestingly, in our data, we also observed that the default mode network showed a similarly high network flexibility [paired t test between the flexibility of the frontoparietal network vs. the flexibility of the default mode network: $t_{(343)} = -0.44$, $P = 0.66$]. Given the differences between the n-back working-memory task used here and the multitask scenario used in the Cole et al. (31) work, these results indicate that the flexibility of distinct cognitive systems can change depending on the task at hand.

Comparison with Traditional Approaches.

Comparison with alternative parcellations. The n-back task has been studied extensively in the context of traditional activation and connectivity analyses (38, 39), identifying a large (executive) working-memory network dominated by frontal and parietal regions. To relate our results to those established findings, we took the 32 regions reported by Owen et al. (39) and identified corresponding nodes from our partition. This was done by simply calculating the Euclidian distance between our nodes and the reported main voxels of activation by Owen et al. We found 46% of the mapped nodes belonging to the frontoparietal module identified by us, whereas 27% belonged to the somatomotor module and 12% belonged to the frontal module. All comparisons can be found in Table S3.

Comparison with general linear model analyses. To ensure that the connectivity matrices are not dominated by simple coactivation during the task blocks, we have regressed out the task activation using a general linear model (GLM), consistent with our prior work (23, 35, 47, 52). Furthermore, we have performed additional analysis to support our claim that network parameters are not driven by activity magnitude alone. Specifically, we checked for associations between the following three statistics: (*i*) network flexibility during 2-back, (*ii*) the difference between flexibility in the 0-back vs. 2-back tasks, and (*iii*) the contrast estimates derived from classical fMRI GLM analysis. We focus this test on two brain regions that displayed the highest differences in flexibility between the 0-back and 2-back conditions: left inferior parietal cortex [−42 −55 45] and right medial orbital frontal cortex [43 49 −2]. The observed correlation between the β weights for the left inferior parietal cortex and the flexibility during 2-back was $r = -0.046$, $P = 0.902$, whereas the correlation between β weights and flexibility difference was $r = -0.067$, $P = 0.217$. The observed correlation between the β weights for the right medial orbital frontal cortex and the flexibility during 2-back was $r = -0.003$, $P = 0.902$, whereas the correlation between the β weights and flexibility difference was $r = 0.045$, $P = 0.408$. These results suggest that the activity of brain regions is unlikely to be driving the observed changes in network flexibility.

Furthermore, to demonstrate that our behavioral results are independent of activation and explain an additional amount of variance, we used the contrast estimates of the most significant voxel in the brain regions traditionally activated by the n-back task. Specifically, we identified the most significant voxels in the left and right parietal cortex and left and right prefrontal cortex and regressed them against accuracy. In all linear regression models with contrast estimates of right prefrontal cortex at [45 35 30] as the dependent variable [$\beta = -0.023$, $t_{(343)} = -0.417$, $P < 0.677$; left prefrontal cortex at [−48 24 33]: $\beta = -0.04$, $t_{(343)} = -0.742$, $P < 0.459$; right parietal cortex at [45 −43 45]: $\beta = 0.031$, $t_{(343)} = 0.573$, $P < 0.567$; left parietal cortex at [−45 −46 45]: $\beta = -0.011$, $t_{(343)} = -0.204$, $P < 0.839$], we found no significant association with task accuracy.

To further validate that flexibility and integration explain an additional amount of variance in comparison with standard fMRI metrics, we used a standard GLM model to infer which brain areas are significantly associated with accuracy. One voxel cluster in the left motor area centering around [−45 −10 48] survived whole-brain familywise error (FWE) correction (peak voxel at [−45 −10 48]: $T = 4.80$, pFWE = 0.014). Again, we extracted the contrast estimates for this voxel and used them as nuisance covariates in a linear regression model, resulting in only a marginal change in significance level for our reported results [linear regression model with flexibility as dependent variable and contrast estimates from voxel at [−45 −10 48] as nuisance covariates: $\beta = 0.124$, $t_{(343)} = 2.259$, $P < 0.024$; frontal integration as dependent variable and contrast estimates from voxel at [−45 −10 48] as nuisance covariates: $\beta = 0.163$, $t_{(343)} = 2.974$, $P < 0.003$]. Therefore, although network reconfiguration explains a small amount of variance, it has quantifiable advantages over traditional analyses and here offers complementary insights into the neurobiological basis of working memory.

Classical Graph Metrics. The application of graph theory allows for the investigation of diverse aspects of network organization. We have focused on community detection, which has been extended to the temporal network scenario, whereas many other graph statistics have not. This extension is built on mathematical machinery that can enhance statistical power in uncovering meaningful (rather than spurious) changes in networks across time. Static graph statistics do not have these same statistical advantages when applied independently to networks extracted from individual time windows. Despite their statistical limitations,

however, we have now also applied static graph statistics to the temporal network data to enable a comparison between these statistics and the dynamic network flexibility. Classical graph statistics such as the weighted path length and weighted clustering coefficient show an oscillatory pattern across the experimental session that is consistent with that observed for network flexibility (Fig. S4). The clustering coefficient is highest between task blocks and lowest within task blocks, whereas the path length is longest between task blocks and shortest within task blocks. These results support the view that, within task blocks, network reconfiguration mainly takes place between modules, thus resulting in a lower clustering coefficient and an increased path length. Conversely, between task blocks, network reconfiguration mainly takes place as local rearrangements within modules.

SI Methods

Participants. A group of 344 healthy volunteers (180 women; mean age, 33; range, 18–51 y) were recruited as part of a multicenter study conducted in the cities of Mannheim, Berlin, and Bonn, Germany. All participants provided informed written consent for a protocol approved by the respective ethics committees. Exclusion criteria included a lifetime history of significant general medical, psychiatric, or neurological illness, prior psychotropic pharmacological treatment, head trauma, and the presence of a first-degree relative with a history of psychiatric illness.

Data Acquisition and Preprocessing. Data were preprocessed as previously described (47). In short, BOLD fMRI was performed on three identical scanners (3-T Siemens Trio) in Mannheim, Bonn, and Berlin, Germany. At all sites, identical sequences and scanner protocols were used. Before the acquisition of functional images, a high-resolution T1-weighted 3D MRI sequence was conducted [magnetization-prepared rapid-acquisition gradient echo; slice thickness, 1.0 mm; field of view (FoV), 256 mm; TR = 1,570 ms; echo time (TE) = 2.75 ms; inversion time = 800 ms; α = 15°]. Subsequently, functional data were acquired using an echo-planar imaging sequence with the following scanning parameters: TR/TE = 2,000/30 ms; α = 80°; 28 axial slices (slice thickness = 4 mm + 1-mm gap); descending acquisition; FoV, 192 mm; and acquisition matrix, 64 × 64.

Image preprocessing was done using SPM and following a standard routine: all images were realigned to the first image of the time series, slice-time corrected, spatially normalized to the Montreal Neurological Institute template (resulting voxel size, 3 mm^3), and spatially smoothed with a 9-mm FWHM Gaussian kernel. For each region of interest, the mean time series was extracted and corrected for signal from white matter and cerebrospinal fluid as well as the six head motion parameters. After removal of the task effect by regression (47), the time series was high-pass filtered at a frequency of 0.008 Hz.

Neuropsychological Testing. Trained psychologists administered several neuropsychological tests to each subject while outside the scanner. These tests included the German translation of the digit span test (53) and the trail-making test (54).

Details of the fMRI Task. Subjects underwent scanning while performing a traditional visual *n*-back paradigm in which a diamond-shaped stimulus containing a number from 1 to 4 was presented every 2 s (Fig. 1*A* in the main manuscript and Fig. S5). In the 0-back condition, subjects were required to press the button on the response box corresponding to the number currently displayed on the presentation screen. In the 2-back condition, subjects were required to press the button on the response box corresponding to the number presented two stimuli before the number currently displayed on the presentation screen. Stimuli were presented in blocks of either 0-back or 2-back conditions, without any additional control condition. In each condition block, a stimulus was presented 14 times. Each condition block was repeated four times in an interleaved manner: a 0-back block was followed by a 2-back block, which was followed by a 0-back block, which was followed by a 2-back block, and so on. Task performance was measured by both accuracy (defined as the percentage of correct answers) and reaction time (defined as the length of time from stimulus onset to button press) for each condition separately.

Estimating Networks of Functional Connectivity. After preprocessing, the mean time series in 5-mm spheres around coordinates defined by ref. 36 were extracted. Because the template defined by Power et al. falls short on providing coverage of the hippocampus, amygdala, and nucleus accumbens, we manually added bilateral coordinates for these three regions based on three metaanalysis articles (55–57).

Using a sliding time window with a length of 15 volumes and no gap between windows, we use the Morlet wavelet transform to estimate the functional connectivity between each pair of brain regions, as described previously (3). We note that, due to the short time intervals of only 30 s and due to our TR of 2 s, we restricted our analysis to the wavelet scales corresponding approximately to the frequency band of 0.08–0.15 Hz. For each subject, this procedure yielded 114 weighted matrices describing the temporal evolution of functional connectivity across the task.

Identifying Putative Functional Modules. For each subject, the resulting matrices were partitioned into time-respecting modules using a multilayer-community detection algorithm introduced and extensively described in ref. 6 and first applied to neuroimaging data in ref. 3. In short, for each subject, the 114 weighted adjacency matrices can be combined to form a rank-3 adjacency tensor $\mathbf{A}$ that can be used to represent time-dependent or multilayered networks. One can thereby define a "multilayer modularity" as follows:

$$Q = \frac{1}{2\mu} \sum_{ijlr} \{(A_{ijl} - \gamma_l P_{ijl})\delta_{lr} + \delta_{ij}\omega_{jlr}\}\delta(g_{il}, g_{jr}), \qquad \text{[S1]}$$

where the adjacency matrix of layer I has components A_{ijl}, the element P_{ijl} gives the components of the corresponding layer l matrix for the optimization null model, γ_1 is the structural resolution parameter of layer l, the quantity g_{il} gives the community assignment of node i in layer l, the quantity g_{jr} gives the community assignment of node j in layer r, the element ω_{jlr} gives the connection strength (i.e., an "interlayer coupling parameter," or "temporal resolution parameter") from node j in layer r to node j in layer l, the total edge weight in the network is $\mu = (1/2)\sum_{jr} k_{jr}$, the strength (i.e., weighted degree) of node j in layer l is $k_{jl} = k_{jl} + c_{jl}$, the intralayer strength of node j in layer l is $k_{jl} = \sum_i A_{ill}$, and the interlayer strength of node j in layer l is $c_{jl} = \sum_r \omega_{jlr}$.

This procedure yields for every region and every time window a community assignment, which indicates the module allegiance.

Maximizing this modularity quality function is NP-hard, and we therefore use a Louvain-like locally greedy heuristic algorithm (50) to seek the optimal modularity index Q. Due to the heuristic nature of the algorithm and to the near degeneracy of the optimization landscape of the multilayer modularity quality function, each independent run of the algorithm provided slightly different partitions of network nodes into communities across the 114 time slices (or network layers). Therefore, we repeated the modularity optimization procedure using a Louvain-like locally greedy algorithm 100 times for each subject. For each repetition, we calculated a flexibility change matrix $\mathbf{F}_{\Delta}$ whose binary elements $\mathbf{F}_{\Delta i,j}$ indicate whether node i changes it module allegiance at the transition j between two consecutive time

windows. Averaging $\mathbf{F}_{\Delta}$ over all repetitions of the modularity optimization, we obtained the average flexibility change matrix for each subject, $\mathbf{F}_{\Delta}$ whose elements $\mathbf{F}_{\Delta i,j}$ estimate the probability that a brain region changes its allegiance to putative functional modules between any two consecutive time windows.

Because dynamic community detection techniques are relatively new, it is important to consider the ability of these techniques to robustly uncover meaningful temporal variations in network organization. The methodological advances used in this work are based on the dynamic community detection techniques, which were developed in the last few years (6), and have since been tested and validated in a wide variety of simulated and empirical scenarios. In the original paper (6), the methods were tested on two different kinds of social networks, and results were consistent with prior knowledge regarding these systems. In a following methods paper (25), we stringently evaluated the methodological choices required to robustly detect dynamic community structure in simulated and empirical data. In that paper, we used simulated data from Kuramoto oscillators (for which there is a large literature illustrating their utility as "neural state" nodes; see, for example, ref. 58 and references therein) on known community structure and demonstrated the ability of the computational techniques to successfully recover that structure. In that paper, we also developed a framework of null model testing for statistical inference in the context of neuroimaging data. Finally, dynamic community detection methods have further been used in the context of human motor skill learning (3) and lexical processing (59). We build on all of this prior validation (both simulated and empirical) and statistical method development in the current manuscript.

Nevertheless, it would be interesting in future to construct a simulated (neural mass) model with biologically realistic temporal variations in community structure specifically inspired by the *n*-back working-memory task. The reason we have not done so in this work is that the precise temporal dynamics of this system is difficult to infer from either a theoretical or an experimental viewpoint for three reasons. First, activation studies and meta-analysis of these tasks (39) usually investigate main effects of working-memory load and not within-load dynamics let alone per-trial effects in fMRI data. Second, per-trial effects are smeared by hemodynamics and therefore difficult to infer from the data. Third, the main effect of task was removed from the data to not confound network measures with large-scale block (co)activations, as has been done previously (e.g., see ref. 23). As a result of these three points, it is arguably premature to establish a good neuronal state model for these specific dynamics at this point. Instead, we base our confidence in the reported results on the previous extensive validations and methodological advances of dynamic community detection techniques (of which time-dependent flexibility estimates are a direct mathematical extension) discussed in the previous paragraph.

Subject-Level and Group-Level Analysis of Putative Functional Modules. To find a consensus partition S that is most representative of a number n of given partitions $C_1, C_2, \ldots, C_n$, we follow the procedure outlined in ref. 25. Specifically, we computed for each partition $C_1, C_2, \ldots, C_n$ its modular allegiance matrix $\boldsymbol{T}$ whose binary elements T_{ij} indicate if two nodes i and j have been assigned to the same module or not. Summing up all modular allegiance matrices, we obtained the consensus matrix T_{cons} whose elements indicate how often two nodes have been assigned to the same module over a set of matrices. To account for noise, only matrix elements whose values were larger than expected in a random network null model were taken into account. In particular, for each of the $C_1, C_2, \ldots, C_n$ partitions, we reassigned nodes uniformly at random to the n communities of mean size s that are present in the selected partition. For every pair of nodes i and j, we let T_{ij}^r be the number of times these two nodes have been assigned to the same community in this permuted situation. The values T_{ij}^r then form a distribution for the expected number of times two nodes are assigned to the same partition. To be conservative, we remove such "noise" from the original nodal association matrix $\boldsymbol{T}$ by setting any element T_{ij} whose value is less than the maximum entry of the random association matrix to 0.

By maximizing a single-layer modularity quality function 100 times on the thresholded consensus matrix T_{cons}, we obtained a consensus partition S that is most representative of the initial partitions $C_1, C_2, \ldots, C_n$. Note that the single-layer modularity quality function can be defined as follows:

$$Q_0 = \sum_{ij} [A_{ij} - \gamma P_{ij}]\,\delta\left(g_i, g_j\right), \qquad \textbf{[S2]}$$

where node i is assigned to community g_i, node j is assigned to community g_j, the Kronecker delta $\delta(g_i,g_j) = 1$ if $g_i = g_j$ and it equals 0 otherwise, γ is a resolution parameter (which is called a "structural resolution parameter"), and P_{ij} is the expected weight of the edge connecting node i to node j under a specified null model.

This procedure can be repeated iteratively, so that repeated optimizations of the modularity quality function of the consensus matrix T_{cons} return a single optimal consensus partition S, which partitions brain regions into representative putative functional modules that we interpret as cognitive systems (25).

To specifically find a community structure that is representative of either the 0-back or the 2-back condition, we applied a three-step procedure.

Step 1: For each subject and time window, we calculated the consensus partition over the 100 optimizations of the multilayer modularity quality function. This procedure yielded a single representative partition for each window for each subject.

Step 2: We computed a representative partition for a given time window by calculating a consensus partition for that window over the partitions obtained for each subject in step 1.

Step 3: To find the consensus partition for each state, we computed the consensus partition for all windows that either contained more than 75% of 0-back data or contained more than 75% of 2-back data.

Determining Integration Between Network Modules. A module's integration with other modules can be computed from the modular allegiance matrix T as described earlier. Integration is defined as the average value of module allegiance elements not in the same module and is an indicator of how much modules interact or integrate with each other. Formally, given a partition $C = \{C_1, \cdots, C_m\}$ of brain regions into m modules. Then,

$$I_{k,l} = \frac{\sum_{i \in C_k, j \in C_l} T_{ij}}{|C_k||C_l|}, \qquad \textbf{[S3]}$$

is the interaction strength between modules C_k and C_l, where $|C_k|$ is the number of nodes in C_k and $1 \le k, l \le m$. To compute the average integration between two different modules ($k \neq l$), we calculate the normalized interaction strength:

$$RI_{k,l} = \frac{I_{k,l}}{\sqrt{I_{k,k} I_{l,l}}}, \qquad \textbf{[S4]}$$

which accounts for differences in module strength.

This definition of integration is flexible in the sense that the integration value can be used to measure different properties of the system, depending on how the modular allegiance is con-

structed. For example, module allegiance matrices constructed over time windows provide information regarding the temporal consistency of modular structure and intermodular integration. In *Results*, *Dynamics of Flexibility*, we calculated integration from a group consensus partition constructed over subjects (see Fig. 2*A* in the main manuscript and step 2 in the previous section). In particular, for each time window, we obtained a group consensus partition that is most representative of the whole group's modular composition in a specific time window. This formulation of the data enabled us to address the temporal consistency of integration between putative functional modules or cognitive systems as subjects performed the *n*-back task.

In *Results*, *Role of Frontal Systems in Executive Functioning*, we were instead interested in addressing individual variation in intermodule integration over subjects. To relate integration to individual differences in behavior, we therefore calculated integration from an optimization consensus partition constructed for each time window and each subject (see step 1 in the previous section). In particular, for each time window, we obtained a consensus partition per subject over the 100 optimizations of the multilayer modularity quality function. This formulation of the data enabled us to address the intersubject variation in time-dependent integration between putative functional modules identified as network communities by uncovering individual differences in time-dependent network configuration.

SI Discussion

Traditional activation measures are and have been critically important for our understanding of the role of brain regions in cognitive processes. However, these approaches are increasingly complemented by connectivity-based approaches, which can provide direct insight into the nature of the underlying network dynamics that allow for behavioral adaptation (60). Indeed, connectivity analyses, and more complex measures of the dynamic reconfiguration of networks in face of different task demands, are not competitive with activation studies but provide very complementary insights that directly address the underlying mechanisms of cognitive processes (61). For example, although classical GLM-based approaches are often interpreted as indicating functional associations between regions, connectivity analyses provide direct evidence of neurophysiological mechanisms defining the roles of brain networks in cognition (2). Thus, the current work can be seen as a direct validation of the role of frontal regions in adaptive behavior, and as clarifying the mechanism of this role as based on dynamic changes in functional connectivity.

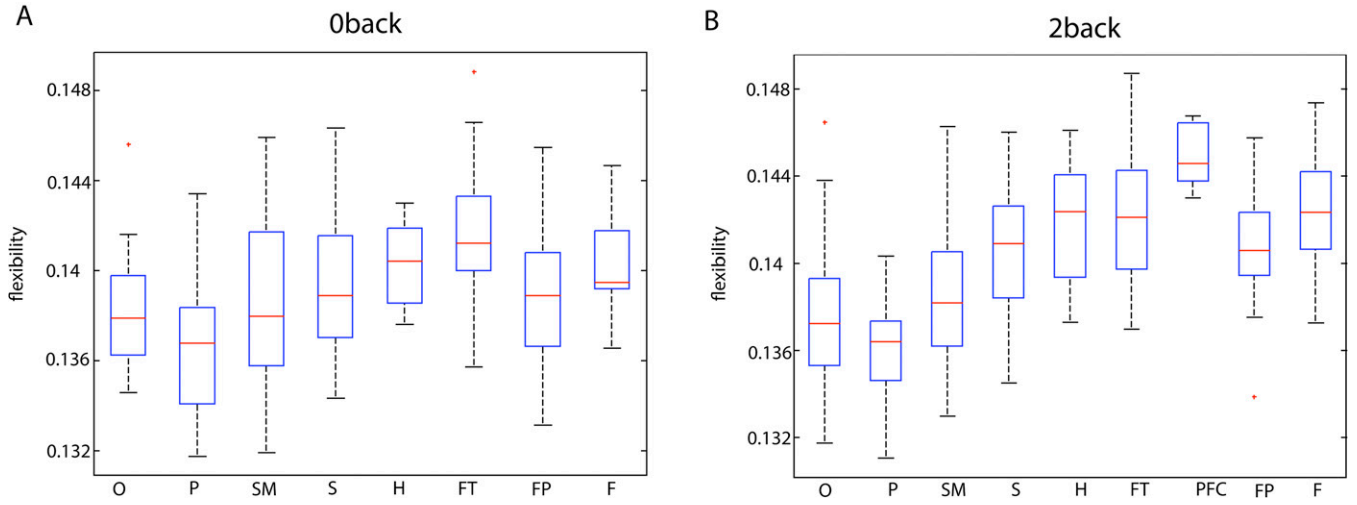

Fig. S1. Distribution of flexibility across cognitive systems. (*A*) The flexibility during 0-back is different across network modules, with modules incorporating frontal nodes showing a higher flexibility than modules lacking frontal nodes. (*B*) The distribution of flexibility is even more pronounced during the 2-back condition, again with frontal modules showing higher flexibility than nonfrontal modules. Module labels are as follows: F, frontal; FP, frontal-parietal; FT, frontotemporal; H, hippocampal; O, occipital; P, parietal; PF, right prefrontal; S, subcortical; SM, somatomotor.

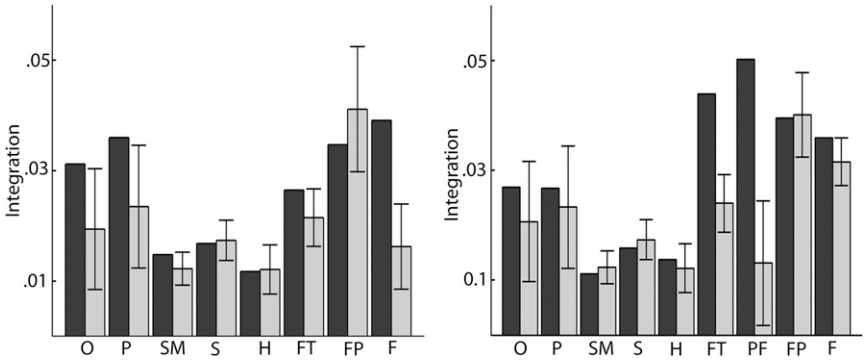

Fig. S2. Distribution of integration across cognitive systems. Integration of different cognitive systems during 0-back (*Left*) and 2-back (*Right*). Black columns indicate original data; gray columns indicate integration from 1,000 permutations of consensus matrix labels. Error bars indicate SD over 1,000 permutations. Module labels are as follows: F, frontal; FP, frontal-parietal; FT, frontotemporal; H, hippocampal; O, occipital; P, parietal; PF, right prefrontal; S, subcortical; SM, somatomotor.

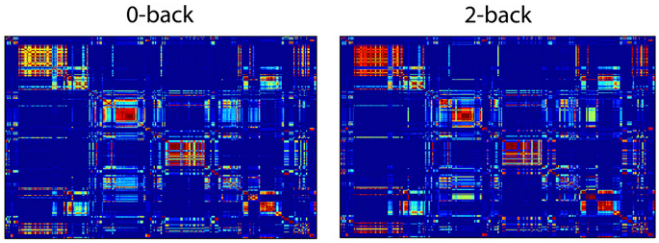

Fig. S3. Community structure during 0-back and 2-back. To optimally visualize the differences in community structure between 0-back and 2-back conditions on a node-to-node basis, we have adapted the original node order presented in an earlier figure to the node order published by Power et al. (36).

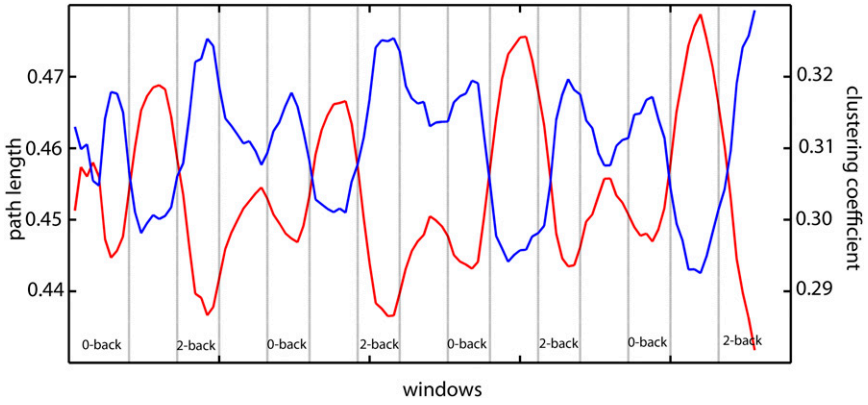

Fig. S4. Classical graph metrics. The mean weighted clustering coefficient (red) and pathlength (blue) for functional networks extracted from overlapping time windows. Values are averaged over subjects. Note that each functional networks was normalized by dividing each edge weight by the mean edge weight in the network; this procedure ensured that observed changes in the statistics were not driven by changes in mean edge weight, but by specific changes in the network topology. We observe an oscillatory pattern in these statistics that is consistent with that observed for network flexibility in the main manuscript.

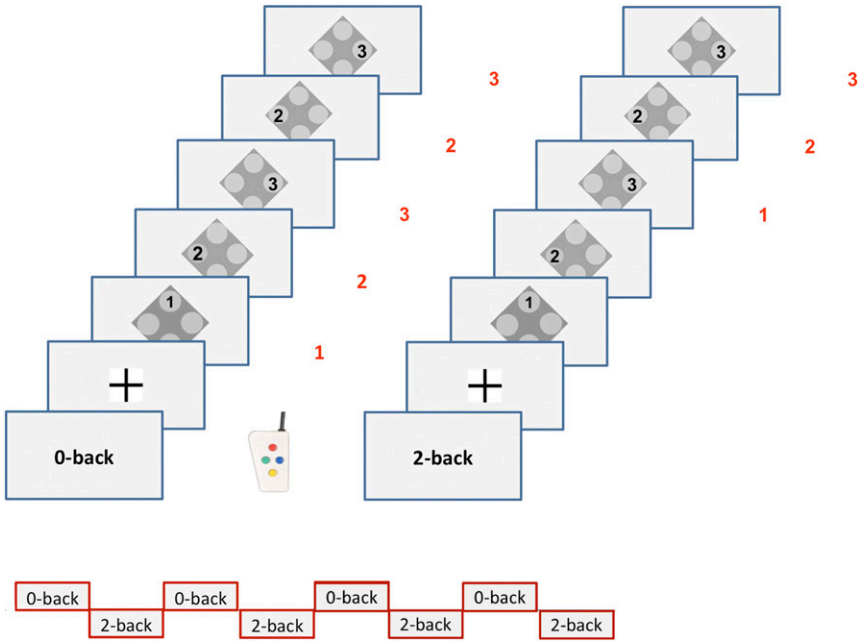

Fig. S5. Details of *n*-back paradigm. Stimuli were presented in blocks of either 0-back (*Left*) or 2-back (*Right*) conditions, without any additional control condition. In the 0-back condition, subjects were required to press the button on the response box corresponding to the number currently displayed on the presentation screen (red numbers next to screen images on the *Left*). In the 2-back condition, subjects were required to press the button on the response box corresponding to the number presented two stimuli before the number currently displayed on the presentation screen (red numbers next to screen images on the *Right*). Each condition block was repeated four times in an interleaved manner as shown on the *Bottom*.

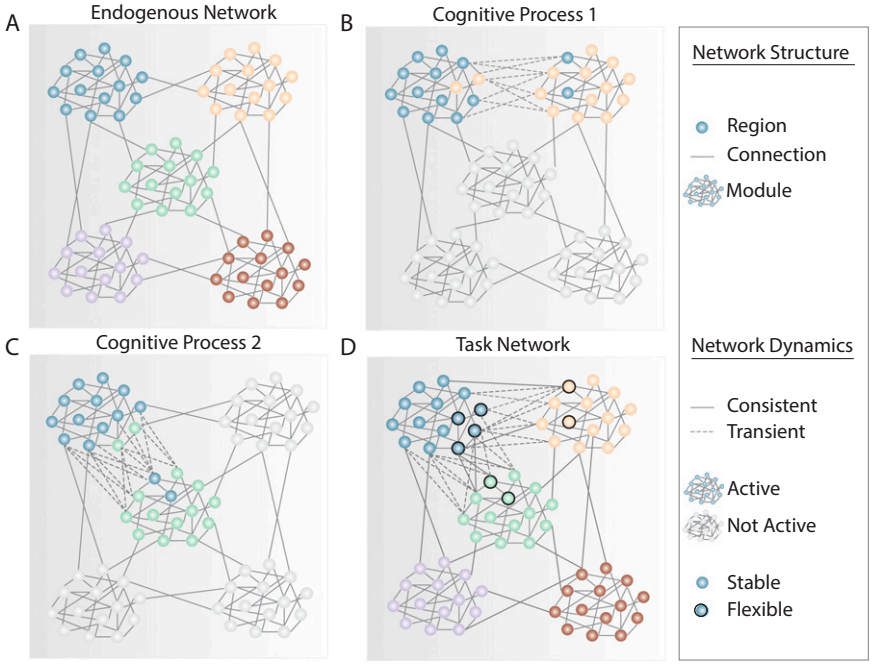

Fig. S6. Schematic of circuit dynamics during task execution. (*A*) At rest, brain functional networks are characterized by network modules, or putative cognitive systems, which contain sets of brain regions that are coherently active with one another (36, 37, 62). (*B* and *C*) A cognitive task paradigm may elicit several cognitive processes, during which modules may interact transiently to share information with one another or enable coherent information processing (2, 40). (*D*) The network dynamics of the task paradigm can be summarized by the flexibility of individual brain regions, which have partnered across modules, and the integration between modules that have been transiently coupled (3, 24).

Table S1. Comparison of systems identified by Power et al. (36) and modules during 0-back

	Occipital		Parietal		Somatomotor		Subcortical		Hippocampal		Frontotemporal		Frontoparietal		Frontal		No module		Sum
System title	No.	%	No.	%	No.	%	No.	%	No.	%	No.	%	No.	%	No.	%	No.	%	No.
"Uncertain"	11	42	0	0	0	0	2	4	4	40	12	44	0	0	0	0	3	16	32
"Sensory/somatomotor hand"	0	0	0	0	29	60	0	0	0	0	0	0	0	0	0	0	1	5	30
"Sensory/somatomotor mouth"	0	0	0	0	1	2	4	9	0	0	0	0	0	0	0	0	0	0	5
"Visual"	6	23	25	86	0	0	0	0	0	0	0	0	0	0	0	0	0	0	31
"Auditory"	0	0	0	0	1	2	11	24	0	0	0	0	0	0	0	0	1	5	13
"Default mode"	1	4	3	10	0	0	0	0	4	40	11	41	33	61	1	9	5	26	58
"Memory retrieval"	0	0	0	0	1	2	0	0	2	20	0	0	4	7	0	0	0	0	7
"Cingulo-opercular task control"	0	0	0	0	7	15	6	13	0	0	0	0	0	0	1	9	0	0	14
"Frontoparietal task control"	1	4	0	0	0	0	0	0	0	0	2	7	15	28	1	9	6	32	25
"Salience"	0	0	0	0	3	6	4	9	0	0	0	0	1	2	8	73	2	11	18
"Subcortical"	0	0	0	0	0	0	13	28	0	0	0	0	0	0	0	0	0	0	13
"Ventral attention"	0	0	0	0	0	0	6	13	0	0	2	7	0	0	0	0	1	5	9
"Dorsal attention"	3	12	1	3	6	13	0	0	0	0	0	0	1	2	0	0	0	0	11
"Cerebellar"	4	15	0	0	0	0	0	0	0	0	0	0	0	0	0	0	0	0	4
Sum	26		29		48		46		10		27		54		11		19		270

All modules identified by us during 0-back and their corresponding decomposition on the left. The absolute number of correspondence (no.) as well as the percentage of overlap (%) is stated.

Table S2. Comparison of systems identified by Power et al. (36) and modules during 2-back

	Occipital		Parietal		Somatomotor		Subcortical		Hippocampal		Frontotemporal		Prefrontal		Frontoparietal		Frontal		No module		Sum
System title	No.	%	No.	%	No.	%	No.	%	No.	%	No.	%	No.	%	No.	%	No.	%	No.	%	No.
"Uncertain"	11	39	0	0	0	0	2	4	4	40	9	45	3	50	0	0	0	0	3	21	32
"Sensory/somatomotor hand"	0	0	0	0	29	60	0	0	0	0	0	0	0	0	0	0	0	0	1	7	30
"Sensory/somatomotor mouth"	0	0	0	0	1	2	4	8	0	0	0	0	0	0	0	0	0	0	0	0	5
"Visual"	8	29	23	85	0	0	0	0	0	0	0	0	0	0	0	0	0	0	0	0	31
"Auditory"	0	0	0	0	1	2	12	25	0	0	0	0	0	0	0	0	0	0	0	0	13
"Default mode"	1	4	3	11	0	0	0	0	4	40	9	45	1	17	14	39	20	61	6	43	58
"Memory retrieval"	0	0	0	0	1	2	0	0	2	20	0	0	0	0	4	11	0	0	0	0	7
"Cingulo-opercular task control"	0	0	0	0	7	15	6	13	0	0	0	0	0	0	0	0	1	3	0	0	14
"Frontoparietal task control"	1	4	0	0	0	0	0	0	0	0	0	0	2	33	15	42	4	12	3	21	25
"Salience"	0	0	0	0	3	6	5	10	0	0	0	0	0	0	2	6	8	24	0	0	18
"Subcortical"	0	0	0	0	0	0	13	27	0	0	0	0	0	0	0	0	0	0	0	0	13
"Ventral attention"	0	0	0	0	0	0	6	13	0	0	2	10	0	0	0	0	0	0	1	7	9
"Dorsal attention"	3	11	1	4	6	13	0	0	0	0	0	0	0	0	1	3	0	0	0	0	11
"Cerebellar"	4	14	0	0	0	0	0	0	0	0	0	0	0	0	0	0	0	0	0	0	4
Sum	28		27		48		48		10		20		6		36		33		14		270

All modules identified by us during 2-back and their corresponding decomposition on the left. The absolute number of correspondence (no.) as well as the percentage of overlap (%) is stated.

Table S3. Comparison with alternative parcellations

Owen ROI			Nearest ROI of our partition					
x	*y*	*z*	No.	*x*	*y*	*z*	Module	Euclidian distance, mm
28	4	50	264	29	−5	54	Somatomotor	9.90
−26	0	52	261	−32	−1	54	Somatomotor	6.40
−44	−2	38	174	−44	2	46	Frontoparietal	8.94
−2	12	42	213	−1	15	44	Somatomotor	3.74
40	32	30	206	31	33	26	Frontal	9.90
−36	44	20	220	−39	51	17	Frontoparietal	8.19
−44	18	22	176	−47	11	23	Frontoparietal	7.68
−30	18	6	208	−35	20	0	Subcortical	8.06
32	20	4	209	36	22	3	Subcortical	4.58
−36	44	20	220	−39	51	17	Frontoparietal	8.19
10	−66	48	135	11	−66	42	Frontoparietal	6.08
−36	−50	40	259	−33	−46	47	Somatomotor	8.60
40	−48	38	199	33	−53	44	Frontoparietal	10.49
2	−64	−24	246	1	−62	−18	Occipital	6.40
38	20	50	193	32	14	56	Frontal	10.39
0	26	36	216	5	23	37	Frontal	5.92
42	30	24	175	48	25	27	Frontoparietal	8.37
−44	4	32	187	−41	6	33	Frontoparietal	3.74
−40	26	24	201	−42	25	30	Frontoparietal	6.40
−32	42	10	220	−39	51	17	Frontoparietal	13.38
−28	62	−4	78	−18	63	−9	Uncertain	11.22
−30	−54	40	191	−28	−58	48	Frontoparietal	9.17
58	−36	44	190	49	−42	45	Frontoparietal	10.86
30	0	48	264	29	−5	54	Somatomotor	7.87
16	4	56	54	7	8	51	Somatomotor	11.05
0	12	42	213	−1	15	44	Somatomotor	3.74
36	36	24	206	31	33	26	Frontal	6.16
10	−58	54	251	10	−62	61	Somatomotor	8.06
24	−60	52	256	22	−65	48	Frontoparietal	6.71
10	−48	64	22	10	−46	73	Somatomotor	9.22
−34	−58	42	191	−28	−58	48	Frontoparietal	8.49
42	−50	36	130	47	−50	29	Frontoparietal	8.60

To relate our results to those established findings, we took the 32 regions reported by Owen et al. (39) and identified corresponding nodes from our partition. This was done by simply calculating the Euclidian distance between our nodes and the reported main voxels of activation by Owen et al.